J Therm Anal Calorim (2012) 107:257–263
DOI 10.1007/s10973-011-1924-8

Synthesis and characterization of CeO_2–graphene composite

Mauro Francisco Pinheiro da Silva · Heloisa Cristina de Jesus Fraga da Costa · Eduardo Rezende Triboni · Mário José Politi · Paulo Celso Isolani

Received: 18 November 2010 / Accepted: 16 September 2011 / Published online: 5 October 2011

Abstract The synthesis and characterization of graphite oxide (GO), graphene (GS), and the composites: GS–CeO_2 and GO–CeO_2 are reported. This synthesis was carried out by mixing aqueous solutions of $CeCl_3{\cdot}7H_2O$ and GO, which yields the oxidized composite GO–CeO_2. GO–CeO_2 was hydrothermally reduced with ethylene glycol, at 120 °C, yielding the reduced composite GS–CeO_2. GO, GS ,and the composites with CeO_2 were characterized by CHN, TG/DTG, BET, XRD, SEM microscopy, FTIR, and Raman spectroscopy. The estimation of crystallite size of CeO_2 anchored on GO and on GS by Raman, XRD, and SEM agreed very well showing diameters about 5 nm. The role of particles of CeO_2 coating carbon sheets of GO and GS was discussed.

Keywords Graphene · CeO_2 · Composites · Graphene–CeO_2 · Hybrid materials · Thermal analysis

Introduction

CeO_2-based materials have been extensively studied due to their wide utilization in industrial catalysis [1]. In oxidation reactions the energetic trade off between the enthalpy of formation of CeO_2 and redox potential of the pair Ce(III)/Ce(IV) is the key step for understanding most of redox catalytic mechanisms.

An explorative study on morphology and crystallography of CeO_2 has correlated the particle size of nanoparticles to Ce(III) contents in the oxide. This study proposes that a phase transition from CeO_2 to Ce_2O_3 is responsible for diminishing the size of oxide particles. However, such behavior is significantly observable only at scales below 10 nm [2].

In addition, recent studies have shown the morphologic modulation of catalytic activity of CeO_2 in redox reactions. The mechanism is attributed to higher amounts of Ce(III), in crystallographic sites of CeO_2 and consequent oxygen vacancies generated due to low O_2 pressures during crystallization. Consequently, Ce(III) crystallographic planes (110) and (100) are exposed to minimize the effect of vacancies on structural stability [3–6].

Therefore, controlled synthesis yielding particles of CeO_2 under 10 nm size or with controlled morphology could result in the modulation of the oxide redox potential and in designing specific redox catalysts based both on morphology and particle size. In this way, supporting CeO_2 particles is an appropriate substrate leads to CeO_2 at sub-10 nm scale, avoiding excessive agglomeration of CeO_2 particles.

Graphene (GS), discovered in 2004, can be obtained by an intercalation of HNO_3 in graphite in an oxidative treatment, followed by exfoliation in ultrasound bath in aqueous NH_4OH solution, yielding graphite oxide (GO). High contents of carboxyl groups present on GO sheets are quite appropriate for nucleation of nanocrystals, such as CeO_2. Beyond that, GS has a high surface area, good stability and conductive character due to its resonant sp^2 system, opening interesting potentialities [7]. Composites of GSs with metal oxides have been recently reported concerning basic and technological aspects [7–13].

M. F. P. da Silva · E. R. Triboni · M. J. Politi · P. C. Isolani (✉)
Instituto de Química, Universidade de São Paulo, CP 26077, São Paulo, SP 05513-970, Brazil
e-mail: pcisolan@iq.usp.br

M. F. P. da Silva · H. C. de Jesus Fraga da Costa
Instituto Educacional Oswaldo Quirino, Faculdade de Ciências Farmacêuticas e Bioquímicas, Rua Brigadeiro Galvão 540, Barra Funda, Ltda, São Paulo, SP, Brazil

Experimental details

Synthesis of GO was carried out by chemical exfoliation of graphite using the procedure described by Hammer [13]: 6 g of graphite were dispersed in 400 mL of 1:2 concentrated HNO_3/H_2SO_4. Portions of 1 g $KClO_3$ were added, every hour, for 72 h (ca. 100 g total). Subsequently, pH was adjusted to ca. 3 by addition of $KHCO_3$. The dark green mixture resulting was filtered and washed with 10% HCl. The brown solid was suspended in ca. 4 L of aqueous NH_4OH (pH 10), under ultrasonic bath, for 3 h. This suspension was centrifuged at 3,000 rpm for 10 min. The resulting pellet was discarded and the remaining suspension was centrifuged at 15,000 rpm for 20 min. This solid was re-suspended under ultrasonic stirring for 30 min at pH 7.

Synthesis of GS was carried by the reduction of 1 g of GO in ethylene glycol under solvothermal treatment, at 433 K, for 24 h [14].

Synthesis of CeO_2/GS was carried out by mixing 1 L of aqueous $CeCl_3 \cdot 7H_2O$ (0.3 g mL^{-1}) and a 1 L of aqueous suspension of (2 g L^{-1}) of GO in a separating funnel. After 30 min, the brown colloidal GO–CeO_2 was decanted and centrifuged. The resulting pellet was washed with deionized water, centrifuged three times and then dried at 333 K, for 24 h, yielding GO–CeO_2. The reduction of GO–CeO_2 was carried out using a solvothermal treatment. Typically 1 g of GO–CeO_2 powder was dispersed in 20 mL ethylene glycol, in an ultrasonic bath for 10 min. This dispersion was left at 433 K, for 24 h, in an autoclave capsule, then centrifuged and washed three times (Fig. 1).

Characterizations

The composites were characterized by using elementary analysis (CHN), thermal analysis (TG/DTG), FTIR, and RAMAN spectroscopies, scanning electronic microscopy (SEM), X-ray diffraction (XRD), and N_2 adsorption isotherm (BET analysis). FTIR spectra were registered using a Bomem MB 100 spectrometer. Raman spectra were recorded on a Renishaw mod. 3000 imaging system, equipped with an Olympus microscope, a He/Ne laser (Spectra Physics mod. 127, $\lambda = 632.8$ nm) and a CCD detector. Calculations of average crystallite sizes of CeO_2 using Raman spectroscopy were carried out by the phonon confinement model approach, using the scattering peak at 469 cm^{-1} [15]. SEM images were recorded on a JEOL field emission scanning electron microscope, JSM 7401F using a SEI detector. Surface areas were measured by N_2 adsorption at 77 K, on a Micromeritics ASAP 2400 equipment. Prior to surface area measurements, samples were degassed under vacuum, at 373 K, for 3 h. XRD patterns were recorded in a Miniflex Rigaku diffractometer using Cu Kα radiation ($\lambda = 0.1518$ nm) with Ni filter. Crystallite size calculations through XRD were done using the Sherer equation [16]. Experimental FWHM of diffraction lorentzian-fitted peaks of CeO_2 in composites were corrected by subtracting the broadening of standard CeO_2, using the relation $L^2 = (L_{sam})^2 - (L_{st})^2$.

Results and discussion

Synthesis of GO and GS have been already discussed in the literature [14]. Mixing aqueous solution of $CeCl_3$ and dispersion of GO yielded a grayish-brown solid that was precipitated quantitatively. The reaction is attributed to the binding of Ce(III) to carboxyl groups of GO forming a salt-like aggregate in which sheets of GO are agglomerated with consequent precipitation of colloidal brown solid. The brown coloration, upon solvothermal reduction in ethylene glycol, turns to deep black, suggesting the formation of GS.

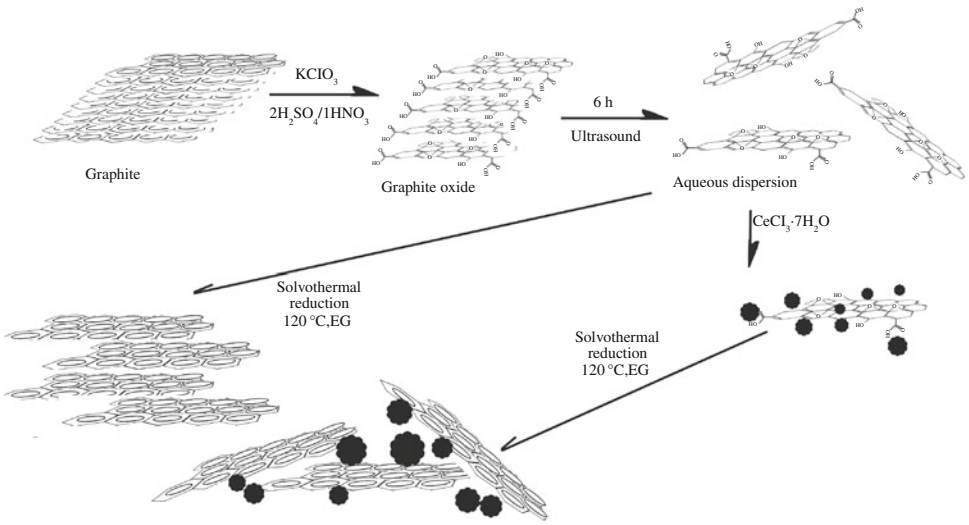

Fig. 1 Illustration of synthetic rout

Both GO and GO–CeO_2 show no conductive properties whereas, after solvothermal reduction, the respective samples GS and GS–CeO_2 show good conductivity and sheet resistance as low as $\sim 4\ \Omega$.

CHN analyses of GO, GS, GO–CeO_2, and GS–CeO_2 are shown in Table 1. As expected, GO holds high amounts of oxygen as carboxyl, epoxides, and alcohol groups [14]. Once reduced solvothermically in ethylene glycol, a dramatic increase of carbon contents takes place. Calculated contents of oxygen from analysis of CH in samples showed 20.8% for GS and 48.4% for GO. These percentages correspond to 5C:1O in GS, against 1.3C:1O in GO. In accordance to thermogravimetric analysis (discussed below) the percentages of C in analysis of CH of GO–CeO_2 are very low. This effect was attributed to the CeO_2 protection: carbon sheets of GO are protected against atmospheric O_2 diffusion and subsequent burning, even at high temperatures. GS–CeO_2, in turn, shows 46% of carbon content. This result allowed an estimation of CeO_2 content in GS–CeO_2 as about 64% in weight, which agrees with the values obtained by TG.

Thermal analysis of GO, GS, GO–CeO_2, and GS–CeO_2 in air, are shown in Fig. 2. Except for GO–CeO_2, all decomposition profiles could be understood as consequences of the oxidation states of carbon structures (GO or GS). GO shows one narrow decomposition process at 473 K and a little mass loss at 873 K, attributed to GS formation, along with burning of GO by dehydration of carboxyl and epoxide groups. GS, in turn, shows one quite narrow decomposition event at ca. 668 K with almost 100% of mass loss. The temperature in which decomposition of carbon sheets takes place is related to the integrity of the sp^2 system. GO has a broken sp^2 system. In this situation, the thermal stability of carbon sheets is poor and GO decomposes totally at a quite low temperature with little residual GS. Once solvothermally reduced, the system recovers the integrity of the sp^2 system. This fact leads to restoring the additional thermal stability; therefore, the temperature of decomposition of GS sheets is high. It should be emphasized that thermal decomposition of GS happens through more than one event.

The composite GS–CeO_2 degrades through three events. The first, starting at ca. 600 K, is attributed to a loss of residual oxygen, merging neighboring sp^2 centers. The next two events happen at 628 and 693 K and are attributed to GS structure decomposition. GO–CeO_2, on the other hand, is not totally decomposed. Instead of a catalytic combustion of oxidized GO sheets, a protection by CeO_2 occurs. The thermal behavior of GO–CeO_2 makes evident this phenomenon. Instead of the quick two-step decomposition showed by GO, GO–CeO_2 shows a fast dehydration followed by a small and gradual mass loss up to 1,500 K. It is proposed that the coating CeO_2 particles prevent burning of carboxylated sheets. This was attributed to the bond of CeO_2 to carboxyl groups, which lowers the probability of atmospheric oxygen getting in touch with carbon. During the reduction reaction and the consequent formation of graphenic sp^2 systems, sheets' surface energy gets lower. This fact implies a lower affinity between carbon surfaces and CeO_2. This was, therefore, attributed to leeching of CeO_2 particles by ethylene glycol.

Table 1 CHN analysis of CeO_2–graphene composites

Sample	%C	%H	%N
GS–CeO_2	45.92	0.97	0.06
GO–CeO_2	1.15	1.07	0.02
GS	78.55	1.11	0.21
GO	48.91	2.68	0.21

XRD diffratometry of GO, GS, and composites are shown in Fig. 3. In GO, only one diffraction peak (002) at ca. 12° (2θ) attributed to GO, could be found. After solvothermal reduction in ethylene glycol, the XRD pattern shows a broad diffraction peak (002), at ca. 24°, attributed to stacking of GS sheets in a very disordered way (turbostatic) [14]. Positions of diffraction peaks indicate that GO presents a distance of 7.4 Å between sheets, while GS presents only 3.66 Å. This shows that during solvothermal reduction, carboxyl and epoxide groups, present in GO, are reduced yielding sp^2 flat groups, which stack within a smaller distance.

Composites between GO and Ce(III) were idealized as a kind of salt in a first approach. Thus, Ce(III) should be bonded to the carbon structure through carboxyl groups. Moreover, it is thought that, after reduction, carboxyl groups should remain as Ce(III)–OOCR groups. XRD pattern shows, however, that after drying at 330 °C for 24 h, only broad peaks characteristic of fluorite structure of CeO_2 appear. This fact points out the strong driving force for the spontaneous formation of fluorite CeO_2 at quite low temperatures. After solvothermal reduction, XRD of GS–CeO_2 shows the diffraction peaks of fluorite structure and new peaks due to the formation of cerium hydroxycarbonate $CeOH(CO_3)$ [17]. CeO_2 XRD peaks become sharper after solvothermal treatment, suggesting the merging of initial CeO_2 particles. Average crystallite size calculated by Sherer equation ($D = 0.9\ \lambda/\beta\ \cos\ \theta$) on (111) (HKL) peaks [18] was 4.2 nm for CeO_2 in GO–CeO_2 and 5.5 nm for CeO_2 in GS–CeO_2. The (002) diffraction peak of both GS and GO could not be found, probably due to stacking impediment caused by intercalation of CeO_2 particles, as already pointed in the literature for GS anchored Mn_3O_4 [19]. BET surface area analysis for GO, GS, GO–CeO_2, and GS–CeO_2 agree with XRD analysis. Bare GO and GS have surface areas of, respectively, 7 and 5 m^2/g. GS–CeO_2

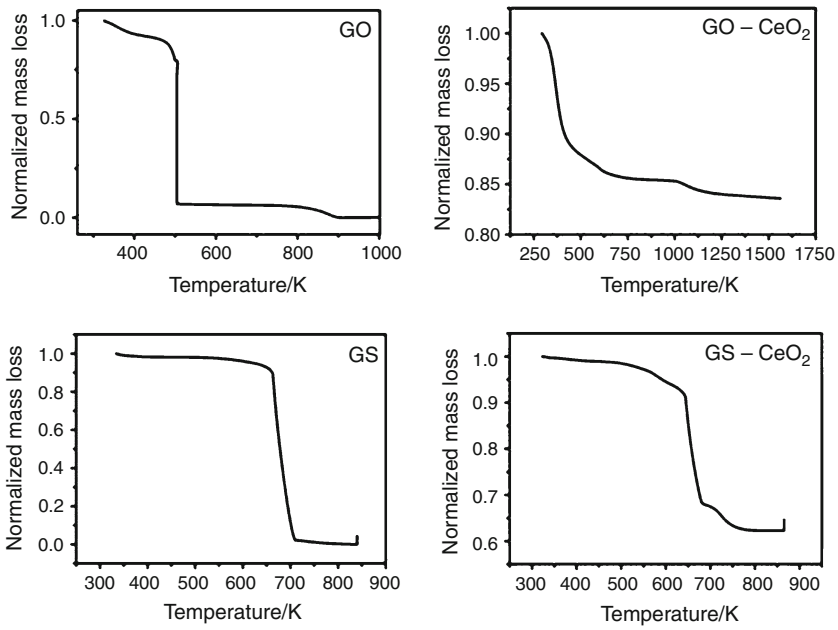

Fig. 2 Thermogravimetric analysis of GO, GS, GO–CeO_2, and GS–CeO_2

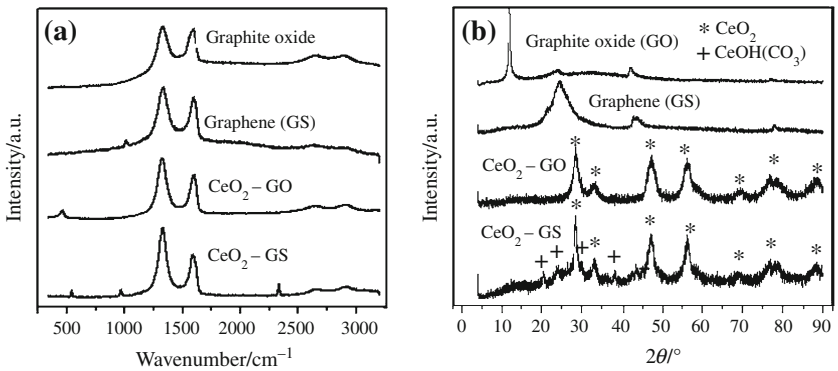

Fig. 3 **a** Raman scattering and XRD patterns of graphite oxide, graphene, GO–CeO_2, and GS–CeO_2. **b** XRD patterns of graphite oxide (GO), graphene sheet (GS) composite between GO–Ce (GO/CeO_2) and the reduced composite (GS/CeO_2)

and GO–CeO_2 have surface areas of, respectively, 90 and 117 m^2/g. It is clear, therefore, the effect of CeO_2 particles as an impediment for stacking GO and GS sheets in the composites.

Raman spectra of GO, GS, GO–CeO_2, and GS–CeO_2 are shown in Fig. 3. The bands G, D, 2G, 2D, and S_3 of GS could be identified, as shown in Table 2. The presence of a D band in all registered spectra suggests that GS obtained from reduction of GO by ethylene glycol, in solvothermal treatment, holds considerable amounts of defects. GO is considered as a small cluster of sp^2 carbons surrounded by sp^3 carbons. Upon reduction under thermal treatment, sp^2 clusters start to merge and form larger clusters. Despite the restoration of the sp^2 system in GS sheets, the intensity of the D relative to G band grows, indicating that no additional organization was gained by reduction of GO on the carbon sheets.

Table 2 Relative intensity of bands D and G of Raman spectrum of synthesized materials

Sample	I(D)/I(G)
GO	1.64
GS	2.14
GS–CeO2	2.08
GO–CeO2	2.14

The presence of CeO_2 is evidenced in GO–CeO_2 by a band at 466 cm^{-1}, corresponding to a symmetrical stretching mode of the vibrational unit Ce–O_8 [4]. The FWHM, ca. 53 cm^{-1}, of this peak fitted with a Lorentzian function was correlated to crystallite size of the oxide through the phonon confinement model [15], yielding a value of 4 nm. In GS–CeO_2 besides GS and CeO_2, [$CeOH(CO_3)$] could be identified. In the composite, however, a clear peak of CeO_2 could not be observed, in contrast to results by XRD. This was attributed to the formation of [$CeOH(CO_3)$] on the surface of particles during reduction. The exciting radiation at 633 nm has not enough penetration power for overcoming the thin layer of cerium hydroxycarbonate that is proposed to be coating the oxide surface.

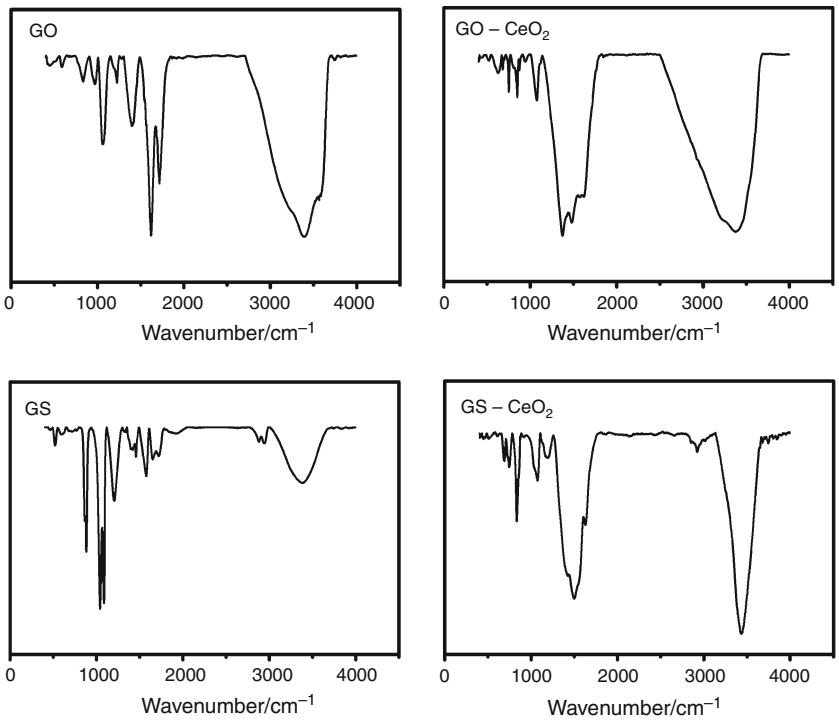

Fig. 4 FTIR spectra of GO, GS, GO–CeO_2, and GS–CeO_2

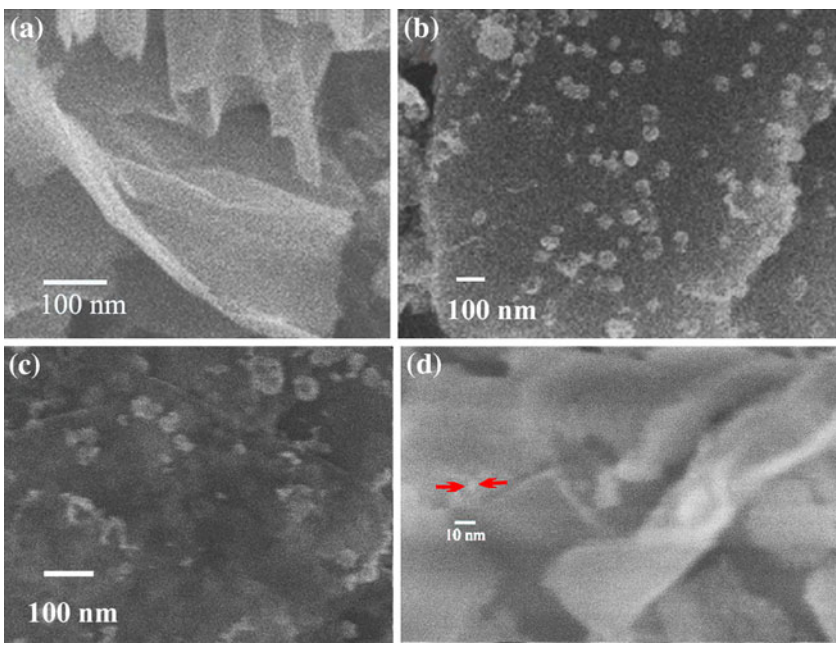

Fig. 5 SEM images of GS (**a**) GS/CeO_2 (**b**–**d**)

FTIR spectra of all prepared materials are shown in Fig. 4. They were interpreted according to the literature [20–22]. GO spectrum presents a strong band in the region of 3,500 cm^{-1} attributed to asymmetric and symmetric stretching of water. Carboxyl groups were identified as a strong and sharp peak in 1,730 cm^{-1}. A peak attributed to symmetric stretching of conjugated alkenes is present in at 1,609 cm^{-1}. Alcohol C–O stretching is identified by a peak at 1,056 cm^{-1} and the epoxide group is identified at 1,080 cm^{-1}.

GS spectra shows, at first approach, small amounts of water, as can be noted by the medium intensity band at ca. 3,500 cm^{-1}. Methylene groups yield strong peaks in the region of 2,880–2,940 cm^{-1}. Knowing that methylene (–CH_2–) has intense bands in that region, the observed low intensities of these peaks suggest a low concentration in the sample. Alcohol groups, as consequence of oxidative treatment of graphite, remain in GS after solvothermal reduction and are identified by the strong peaks at ca. 1,080 cm^{-1}. Aromatic groups are identified by the out-of-

plane C–H vibration, a strong peak at 877 cm^{-1}. Skeletal vibration gives rise to peaks in the region of 1,500 cm^{-1}.

GO–CeO_2 shows interesting features. The most prominent peaks are water at ~3,400 cm^{-1} and the U_3 mode of carbonate ion in the region 1,150–1,800 cm^{-1} as a reaction product of CeO_2 and atmospheric CO_2. A discrete shoulder in 1,730 cm^{-1} and a peak in 1,375 cm^{-1} are attributed to carboxyl groups; the stretching of conjugated double bonds of carbon sheets is present at 1,730 cm^{-1}. Five other peaks attributed to vibrational modes of carbonate ion, at 630, 683, 752, 853, and 875 cm^{-1} could be identified.

The spectrum of GS–CeO_2, in turn, shows the U_3 carbonate mode of vibration in the range 1,260–1,720 cm^{-1}, as well as carboxyl peaks at 1,730 and 1,375 cm^{-1}. Carboxyl peaks are less intense, suggesting low carboxyl group amounts due to reduction of material in the EG solvothermal treatment. The peak intensity of conjugated dienes are also low, suggesting that the reduction treatment decreases these species in the GS sheets. Other five peaks attributed to carbonate were also identified at 630, 683, 752, 853, and 875 cm^{-1}.

SEM analysis of GS and GS–CeO_2 composites are shown in Fig. 5. The quality of obtained images depends on the conductivity of materials, thus, SEM analysis of GO and GO–CeO_2 did not yield good images (not shown), due to the low conductivity of these materials, caused by its broken sp^2 system. GS and GS–CeO_2, on the other hand, have their sp^2 system whole, yielding good images by SEM analysis.

SEM analysis shows that the composite is an aggregate of particles of CeO_2 anchored on GS sheets. Aggregates have ca. 100 nm and individual particles ca. 6 nm diameters, as shown in Fig. 5, in good agreement with XRD and Raman particle size calculations.

Conclusions

The synthesis method here reported produced particles of CeO_2 lower than 10 nm in size coating carbon sheets in both the oxidized and reduced forms of the composites. The agglomeration of carbon sheets is inhibited, thus causing a large surface area of these composites in the solid state.

In an alternate method reported in the literature for GS–CeO_2 GS [23], the synthesis was carried out through addition of solid GO to solution to solution of Ce(III)–polypyrrolidone. Then the mixture was submitted to solvothermal treatment. The XRD pattern presented, however, shows the peak (002) at ca. 12°, which suggests staking of GS sheets at some extent.

The synthesis adopted in this study was carried out by a two-step route. As first, GO was added to Ce(III) solution through aqueous solutions, which ensures large extent of reaction due to high dispersed state of carbon sheets. After isolated, this product's X-ray diffraction patterns did not show evidences of staked carbon sheets. This fact indicates a more intimate interaction between the oxide phase and carbon phase in both GO–CeO_2 and GS–CeO_2 composites. It is important to note that, by adding GO as a solid to $CeCl_3 \cdot 7H_2O$ aqueous solutions, in an ultrasonic bath, the product does not show the same thermal stability as shown by the GO–CeO_2 obtained in this study.

These new materials (both oxidized and reduced composites) have shown remarkable unexpected properties that can be used for technological purposes, such as the thermal stability up to 1,400 °C, in synthetic air, presented by GO–CeO_2. The high surface area presented by composites and conductive character of GS–CeO_2 with can be applied in the construction of electrochemistry sensors.

Acknowledgements The authors wish to thank Lara DC (SESC/LSCP) for his help and support in TG analyses, Ando RA, Serrano, SHP for providing high-purity graphite, CAPES for a doctoral fellowship, and Fantini M.C.A., for the surface area measurements.

References

1. Trovarelli A, Leitenburg C, Boaro M, Dolcetti G. The utilization of ceria in industrial catalysis. Catal Today. 1999;50:353–67.
2. Tsunekawa S, Sahara R, Kawazoe Y, Ishikawa K. Lattice relaxation of monosize CeO_2 nanocrystalline particles. Appl Surf Sci. 1999;152:53–6.
3. Tana, Zhang M, Li J, Li H, Li Y, Shen W. Morphology-dependent redox and catalytic properties of CeO_2 nanostructures: nanowires, nanorods and nanoparticles. Catal Today. 2009;148:179–83.
4. Pinheiro da Silva MF, Soeira LS, Dagasthanli KRP, Martins TS, Cucovia IM, Freire RS, Isolani PC. CeO_2-catalyzed ozonation of phenol: the role of cerium citrate as precursor of CeO_2. J Therm Anal Calorim. 2010;102:907–13.
5. da Silva MFP, Matos JR, Isolani PC. Synthesis, characterization and thermal analysis of 1:1 and 2:3 lanthanide(III) citrates. J Therm Anal Calorim. 2008;94:305–11.
6. da Silva MFP, Carvalho FMS, Martins TS, Fantini MCA, Isolani PC. The role of citrate precursors on the morphology of lanthanide oxides obtained by thermal decomposition. J Therm Anal Calorim. 2010;99:385–90.
7. William S, Hummers Jr, Offeman RE. Preparation of graphitic oxide. J Am Chem Soc. 1958;80:1339–42.
8. Chen S, Zhu J, Huang H, Zeng G, Nie F, Wang X. Facile solvothermal synthesis of graphene–MnOOH nanocomposites. J Solid State Chem. 2010;183:2552–7.
9. Xu C, Wang X, Yang L, Wu Y. Fabrication of a graphene–cuprous oxide composite. J Solid State Chem. 2009;182:2486–90.
10. Zhang K, Dwivedi V, Chi C, Wu J. Graphene oxide/ferric hydroxide composites for efficient arsenate removal from drinking water. J Hazard Mater. 2010;182:162–8.
11. Lu T, Zhang Y, Li H, Pan L, Li Y, Sun Z. Electrochemical behaviors of graphene–ZnO and graphene–SnO_2 composite films for supercapacitors. Electrochim Acta. 2010;55:4170–3.
12. Yao J, Shen X, Wang B, Liu H, Wang G. In situ chemical synthesis of SnO_2–graphene nanocomposite as anode materials for lithium-ion batteries. Electrochem Commun. 2009;11:1849–52.

13. Zhu N, Liu W, Xue M, Xie Z, Zhao D, Hang MZ, Chen J, Cao T. Graphene as a conductive additive to enhance the high-rate capabilities of electrospun $Li_4Ti_5O_{12}$ for lithium-ion batteries. Electrochim Acta. 2010;55:5813–8.
14. Jeong H, Lee YP, Lahaye RJWE, Park M, An KH, Kim IJ, Yang C, Park CY, Ruoff RS, Lee YH. J Am Chem Soc. 2008; 130:1362–6.
15. Nethravathi C, Rajamathi Ml. Chemically modified graphene sheets produced by the solvothermal reduction of colloidal dispersions of graphite oxide. Carbon. 2008;461:994–8.
16. Kosacki I, Suzuki T, Petrovsky V, Anderson HU, Colomban PH. Raman scattering and lattice defects in nanocrystalline CeO_2 thin films. Solid State Ion. 2002;149:99–105.
17. Bärnighausen H, Schiller G. The crystal structure of A-Ce_2O_3. J Less Common Metals. 1985;110:385–90.
18. Guinier A. Theorie et Technique de la Radiocristallographie. 3rd ed. Paris: Dunod; 1964.
19. Wang B, Park J, Wang C, Ahn H, Wang G. Mn_3O_4 nanoparticles embedded into graphene nanosheets: preparation, characterization, and electrochemical properties for supercapacitors. Electrochim Acta. 2010;55:6812–9.
20. D'Assunção LM, Giolito I, Ionashiro M. Thermal decomposition of the hydrated basic carbonates of lanthanides and yttrium. Thermochimica Acta. 1989;137:319–30.
21. Mermoux M, Shabre Y, Russeal A. FTIR AND 13C NMR study of graphite oxide. Carbon. 1991;29:469–74.
22. Nakamoto K. Infrared and Raman spectra of inorganic and coordination compounds. 4th ed. Toronto: John Wiley and Sons; 1986.
23. Wang G, Bai J, Wang Y, Ren Z, Bai J. Preparation and electrochemical performance of a cerium oxide–graphene nanocomposite as the anode material of a lithium ion battery. Scripta Mater. 2011;65:339–42.